# What Balances the Decrease in Net Upward Thermal Radiation at the Surface in Climate Change Experiments?

Jin-Song von Storch*, Michael Botzet and Iris Ehlert

*Max-Planck-Institut fuer Meteorologie, Bundesstrasse 53, D-20146 Hamburg, Germany*

**Abstract:** The direct response of surface fluxes to an increase in green house gas concentration is a decrease in net upward long-wave radiation (NLW). This paper examines the responses of the other three surface fluxes, i.e. the latent heat flux ($H_L$), the sensible heat flux ($H_S$) and the net short wave radiation (NSW), using a set of IPCC AR4 climate experiments performed with the coupled ECHAM5/MPI-OM AO-GCM. In particular, the questions of whether and how these fluxes compensate the warming effect due to a decrease in upward NLW are studied.

Consistent with the earlier studies, the decrease in upward NLW is strongly compensated by an increase in upward $H_L$. By using the IPCC scenarios and a coupled AO-GCM, two new aspects of this compensation are identified. First, the degree of compensation decreases with the rate of increase in GHG concentration. Secondly, the compensation does not work over the North Atlantic, where the decrease in upward NLW develops parallel to a reduction in upward $H_L$. This leads to large increases in the net downward heat flux over the North Atlantic and a reduction of the MOC. The responses in $H_S$ and NSW can further strengthen or suppress the warming effect of NLW, depending on geographical regions considered. There is a general tendency that $H_S$ changes in the same direction as NLW over sea, but in the opposite direction over land. For NSW, the response strengthens the NLW changes over land and suppresses the NLW changes over sea.

## 1. INTRODUCTION

The energy budget at the surface is a fundamental element of climate. Of crucial importance for this budget is the total surface heat flux, which is the sum of the net long-wave thermal radiation (LW), the net short wave solar radiation (SW), the latent heat flux ($H_L$) and the sensible heat flux ($H_S$). We use the convention that downward fluxes are positive and upward fluxes are negative. For changes in fluxes, positive (negative) values indicate an increase in downward (upward) fluxes, or equivalently a decrease in upward (downward) fluxes. If not mentioned otherwise, we will consider the *net* long-wave and short-wave radiation (NLW and NSW) only and will not decompose it into the upward and downward long-wave and short-wave components.

In an equilibrium state, the global integral of the sum NLW+NSW+$H_L$+$H_S$ vanishes, meaning the four fluxes balance each other globally. Increasing greenhouse gas (GHG) concentration perturbs this balance. The size of the imbalance determines the extent to which the surface is heated up. The surface warming directly affects the surface climate. In this sense, understanding how the balance of surface fluxes can be perturbed by an increase in GHG concentration is crucial for understanding and predicting anthropogenic climate changes.

It is well appreciated that a direct response of surface fluxes to an increase in GHG concentration is the decrease in net upward long-wave radiation. An increase in GHG concentration enhances the absorption of the outgoing long-wave radiation from the surface, resulting in surface warming and convective mixing. This in turn leads to a tropospheric warming and an additional decrease in the upward NLW at the surface. What is less clear is whether and how this change in NLW initializes positive or negative feedbacks so that the warming effect of NLW is strengthened or suppressed by responses in NSW, $H_L$ and $H_S$, leading to a stronger or weaker surface warming.

In principle, all three fluxes, $H_L$, NSW, and $H_S$, are able to counteract the warming effect due to the decrease in the upward NLW. A decrease in upward NLW can warm the surface. The warming can enhance evaporation and results in an increase in the upward $H_L$ that partially compensates the warming effect due to the decrease in upward NLW. Furthermore, an increase in tropospheric water vapor can lead to an increase in cloud formation. An increase in cloud cover can reduce the downward solar radiation at the surface, leading to a weakening of the effect of NLW. Finally, if the surface is warmed up faster than the air, there will be an increase in upward $H_S$. In this case, the warming effect of NLW is suppressed by $H_S$.

On the other hand, all three fluxes NSW, $H_L$ and $H_S$ can also act to enhance the warming effect of decreased upward NLW and produce an even larger increase in the total heat flux. A warming induced by decreased upward NLW can lead to a reduction of sea ice that lowers the planetary albedo and increases the downward NSW. Evaporation and from that the upward $H_L$ could decrease, if surface wind speed is strongly reduced. The changes in $H_S$ could be downward, if the air warms up faster than the surface, which could easily happen over the ocean.

*Address correspondence to this author at the Max-Planck-Institut fuer Meteorologie, Bundesstrasse 53, D-20146 Hamburg, Germany; Tel: +49 40 41173 155; Fax: +49 40 41173 366; E-mail: jin-song.von.storch@zmaw.de

1874-2823/08 

Previous studies on surface energy budget [1-5] suggest both positive and negative feedbacks. With respect to globally averaged values, all of these studies identified a decrease in upward NLW as a direct response to an increase in GHG concentration. However, the way how NSW, $H_L$ and $H_S$ respond to changes in GHG concentration are different in different models. Most of the models suggested that the reduced upward NLW is mainly balanced by an enhanced upward $H_L$. But such a role of $H_L$ is not confirmed by the study of Wild *et al*. [4], where the reduced upward NLW is partially compensated by a reduction in NSW due to an increase in cloud amount and atmospheric water vapor. The main discrepancy among the models considered concerns NSW. While some models suggested an increase in incoming solar radiation [1,3], other showed no changes [5] or the opposite [2,4,5].

Given the different results of the previous studies, the present study reexamines the roles of surface fluxes and the feedbacks involved using climate change experiments performed with an improved model. The model considered is the ECHAM5/MPI-OM coupled atmosphere ocean general circulation model (AO-GCM) developed at the Max-Planck Institute for Meteorology. Different from the runs analyzed earlier, the ECHAM5/MPIOM model contributes to the IPCC fourth Assessment Report and belongs in this sense to a new generation of models. Its horizontal resolution, T63 in the atmosphere (and a grid size of about 12 to 150 km in the ocean), is much higher than the R15 resolution in the NCAR and GFDL GCM and the $8^o$ (latitude) x $10^o$ (longitude) grid size in the GISS model considered in [1], the T31 resolution in the CCC GCMII in [2], and the R21 resolution in CSIRO9 GCM in [3]. The only exception is the ECHAM3 model used in [4], who used the T106-resolution. Furthermore, most of the previous experiments are done with an atmospheric GCM coupled to a slab ocean, while the ECHAM5/MPIOM is a fully coupled AO-GCM. No flux corrections are applied for the coupling. Finally, the previous studies focused mainly on $2xCO_2$ experiments, while the experiments with the ECHAM5/ MPIOM are transient runs forced by the greenhouse gas concentrations and aerosol ($SO_4$) concentration resulting from the IPCC AR4 emission scenarios. Thus, the responses in surface fluxes result not only from an increase in GHG concentration, but also from changes in $SO_4$-concentration.

The paper is organized as following. After a short description of the model and experiments in section 2, signatures of surface flux responses to an increase in GHG concentration are identified in section 3. Section 4, 5 and 6 analyze the effects and feedbacks that affect the responses in short-wave radiation NSW, $H_S$ and $H_L$. Of particular concern is the question whether NSW, $H_S$ and $H_L$ will enhance or suppress the warming effect induced by the decrease in upward NLW. Conclusions are given in section 7.

## 2. CLIMATE CHANGE EXPERIMENTS

The climate change experiments considered are carried out with the ECHAM5/MPIOM model. More details concerning the atmospheric component, the ECHAM model, and the oceanic component, the MPIOM model, can be found in [6,7]. The same coupled model is used in [8]. The surface and atmospheric radiation budgets in two earlier versions of the ECHAM model were discussed in [9]. The control run was carried out first using the pre-industrial $CO_2$ concentration. Starting from the control run, the coupled model was forced by the observed anthropogenic (i.e. GHG and sulfate) and natural (i.e. solar and volcanic) forcing from 1860 to 2000, and by the anthropogenic forcing (GHG and sulfate) until year 2100. The 21st century anthropogenic forcing follows the B1, A1B and A2 emission scenarios from the IPCC fourth assessment report. By the end of the 21st century, the $CO_2$ concentration in B1, A1B and A2 scenario reaches 540, 700, 835 ppm, respectively. Both the 20th century run and the 21st century scenario runs are carried out in form of an ensemble with three ensemble members which differ only in initial conditions.

The analysis below concentrates on the 21st century, more precisely on the changes relative to the 20th century. To study the spatial characteristics, differences between the ensemble mean of the last 20 years of the 21st century (2080-2099) and that of the first 20 years in the 20th century (1900-1919) are calculated. The periods are chosen to maximize the signal related to the GHG forcing. The time series are ensemble means of anomalies, which are obtained by subtracting the 20-year means (1900-1919).

## 3. SIGNATURES OF SURFACE FLUX RESPONSES TO AN INCREASE IN GHG CONCENTRATION

All four surface fluxes respond notably to increases in GHG concentration in the scenario runs. The following concentrates on the spatial characteristics of the responses and the balances on global and continental scales.

### a) Spatial Characteristics

The differences of 20-year means for the four flux components, NLW, NSW, $H_S$ and $H_L$ reveal similar structures for different scenarios, but their magnitude increases from B1-, to A1B- and A2-scenario. Consider first the spatial characteristics derived from the A2-scenario runs.

As expected, the response of the thermal radiation is characterized by a decrease in upward NLW almost everywhere on the globe (solid lines and warm colors in Fig. (**1a**)). The largest positive values of about 10 to 20 $W/m^2$ are found over the tropical and subtropical oceans. There are secondary maxima of about 6 to 8 $W/m^2$ over the Southern Ocean around $55^oS$ and over the North Atlantic around $55^oN$. Decreases in the downward NLW (dashed lines and cold colors in Fig. (**1a**)) occur only in limited areas along the Antarctic coast, over the northern North Atlantic and over some land areas.

The largest response of solar radiation (Fig. **1b**) is an increase in downward NSW up to 20 $W/m^2$ near the borders of the present-day sea-ice distribution and a decrease of up to $20W/m^2$ over the tropical Pacific. Apart from these large changes, the incoming NSW is reduced over most of the

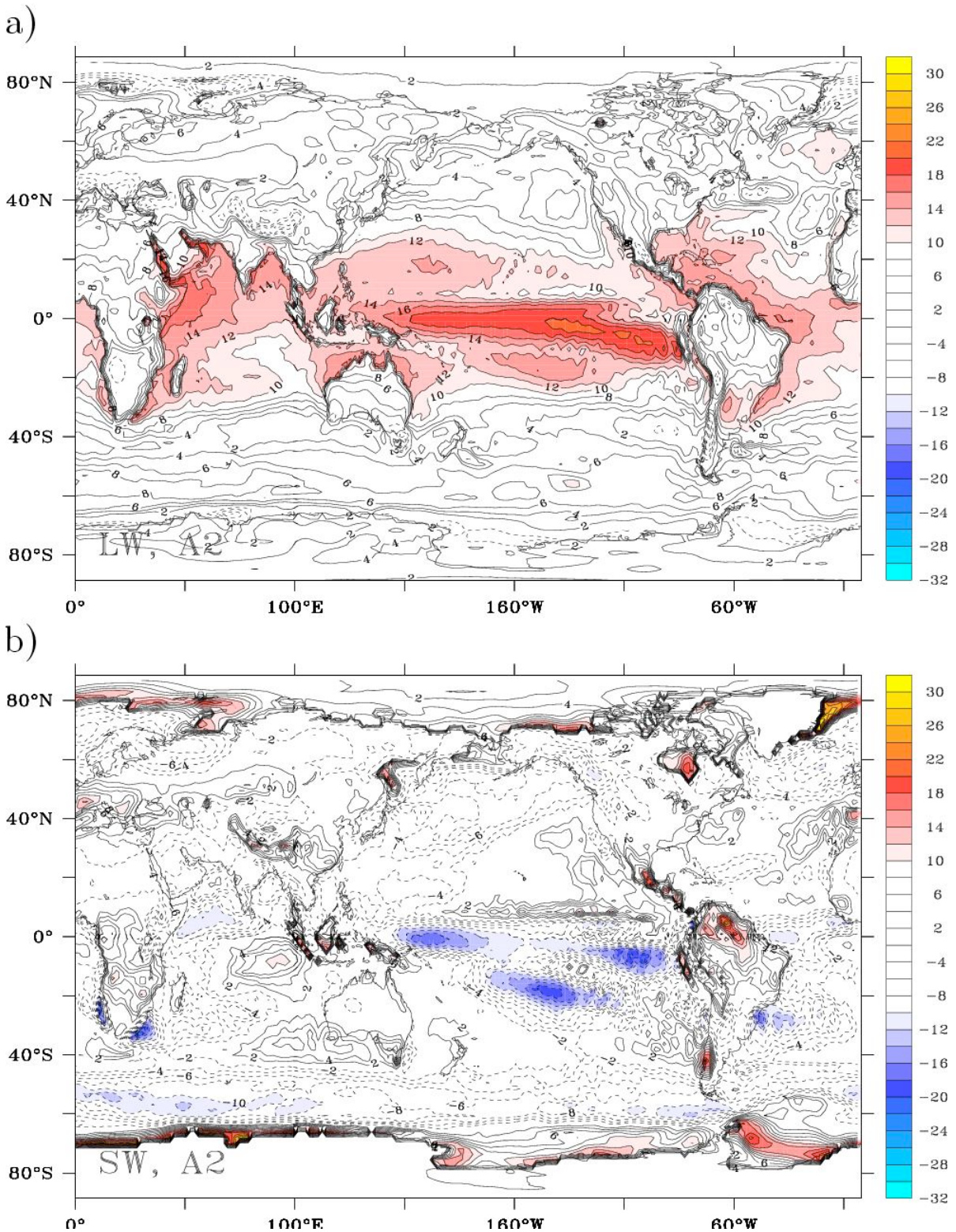


**Fig. (1).** Difference maps for (**a**) long-wave and (**b**) short-wave radiation obtained from the A2 scenario. A difference map represents the difference between the ensemble mean over the last two decades in the 21st century (2080-2099) and the ensemble mean over the first two decades in the 20th century (1900-1919). The unit is $W/m^2$ and the color scale is the same in both panels.

oceans. There are a few regions with an increase in NSW, for instance over central America, the Mediterranean, southern part of Africa and southwest of Australia.

Responses in $H_S$ (Fig. **2a**) reveal a strong land-sea contrast. Generally, there is an increase in downward sensible heat over the oceans, in particular over the mid- and high-latitude oceans, and an increase in upward sensible heat over land.

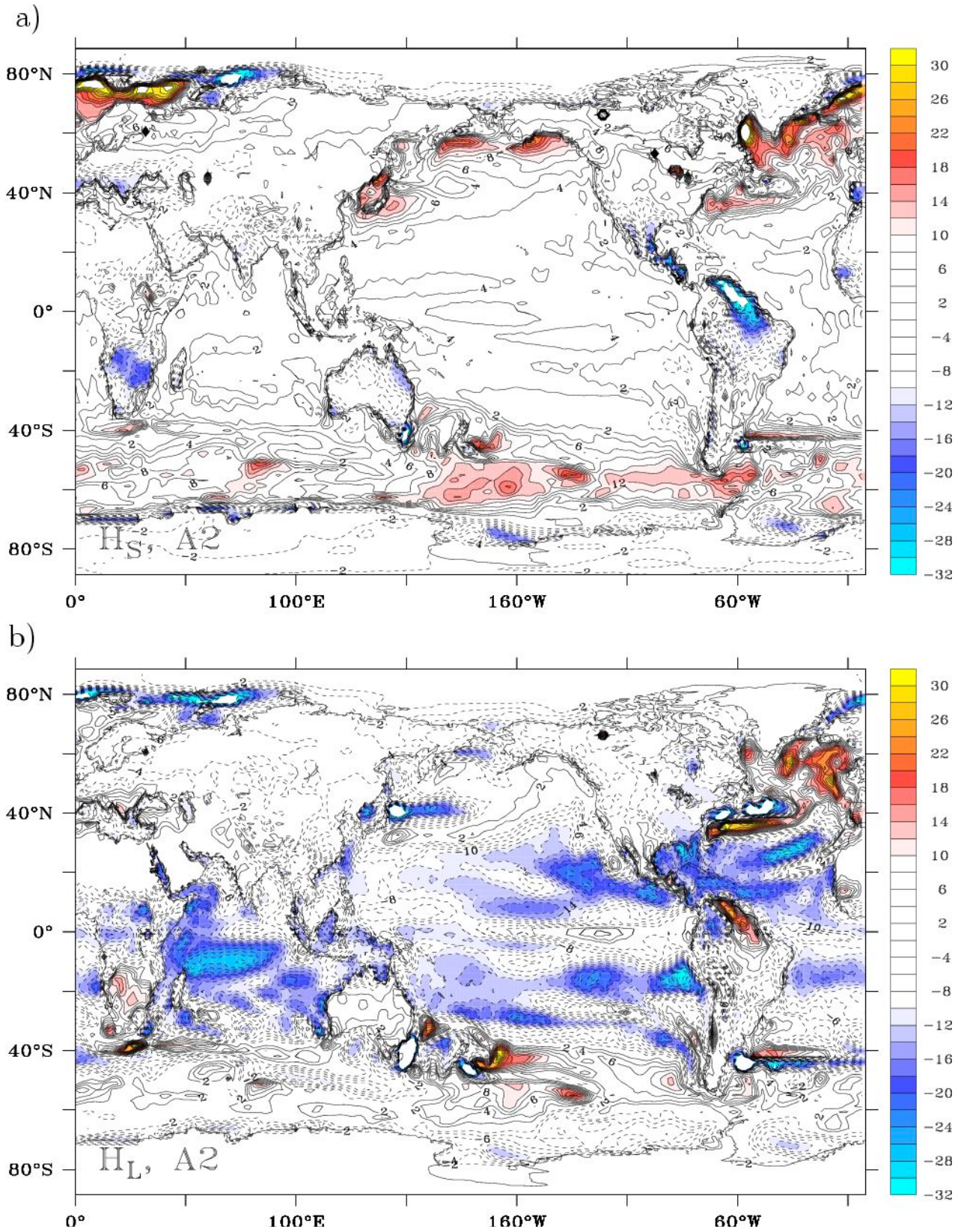


**Fig. (2).** Same as Fig. (**1**), but for (**a**) sensible heat flux and (**b**) latent heat flux.

The difference map for $H_L$ (Fig. **2b**) shows an increase in upward latent heat flux over most of the globe, with the largest values of about 10 to 20 W/m$^2$ over the tropical and subtropical oceans. These changes have about the same magnitude as the changes of the long wave radiation, suggesting a compensation between NLW and $H_L$. Note that even though

large changes of opposite signs are found in the tropics and subtropics for both NLW and $H_L$, the spatial distribution of NLW changes differ notably from that of $H_L$. This difference could be related to the enhanced Hadley circulation associated with an increase in $H_L$. Note also that the compensation does not occur everywhere. There are two exceptions, one in the North Atlantic, where a reduction in upward latent heat flux of about 20 W/m$^2$ and more is found, another over the southern Pacific around 40$^o$S to 60$^o$S with the reduction being somewhat weaker than in the North Atlantic. In both regions, the warming effect of the downward thermal radiation is enhanced, rather than reduced, by the responses in latent heat flux.

The above described spatial features are characteristic not only for the A2-scenario, but also for the A1B- and B1-scenarios. To quantify the similarity between the different maps in A2-scenario and those in B1- or A1B-scenario, the pattern correlation $r_1$

$$r_1 = \frac{< p_i, p_{A2} >}{(< p_i, p_i >< p_{A2}, p_{A2} >)^{1/2}} \quad (1)$$

is calculated, where <,> indicates the scalar product between two fields, $p_{A2}$ denotes the difference map in A2-scenario and $p_i$ with i=A1B, B1 the difference map for the B1- or A1B-scenario. To quantify the strength of the response in A1B- and B1-scenario relative to that in the A2 scenario, the pattern correlation $r_2$

$$r_2 = \frac{< p_i, p_{A2} >}{< p_{A2}, p_{A2} >} \quad (2)$$

is calculated.

The values of $r_1$ shown in Table **1** confirm that the response structures shown in Figs. (**1**,**2**) do not depend on scenarios. The values of $r_2$ show that the amplitudes of these structures increase from B1-, to A1B- and A2-scenario, with the response in the B1-scenario being about 65-70% and that in the A1B-scenario about 90% of that in the A2-scenario.

**Table 1. Pattern Correlation $r_1$ and $r_2$, as Defined in Eq. (1) and Eq. (2).**

| | | NLW | NSW | $H_S$ | $H_L$ |
|---|---|---|---|---|---|
| $r_1$ | B1 | 0.99 | 0.95 | 0.96 | 0.96 |
| | A1B | 0.99 | 0.97 | 0.99 | 0.98 |
| $r_2$ | B1 | 0.63 | 0.67 | 0.71 | 0.69 |
| | A1B | 0.89 | 0.91 | 0.91 | 0.93 |

### b) Balances on Global and Continental Scales

To study the balances on global and continental scales, the four flux components are averaged over the global surface, the ocean and the land areas, for years 2000 to 2100 and for each scenario. To concentrate on the changes, the 20-year means (1900-1919) of the respective area averages in the 20th century are subtracted.

**Table 2. Globally Averaged Changes in NLW and $H_L$ and the Amplitude of $|H_L|$ Relative to NLW in Scenario A2, A1B and B1 at the End of the 21st Century.**

| | A2 | A1B | B1 |
|---|---|---|---|
| NLW | 7.7 | 6.7 | 4.4 |
| $H_L$ | -6.0 | -5.9 | -4.2 |
| NLW/$H_L$ | 0.78 | 0.88 | 0.95 |

The values are obtained by averaging over the last five years shown by the green and black curves in Fig. (**3**).

Fig. (**3**) shows that the flux responses increase with increasing GHG concentration and reach the largest amplitude by the end of the 21st century. There is clear evidence for a compensation of the decrease in upward NLW (green curves) by an increase in upward $H_L$ (black curves). The responses in NLW and $H_L$ over sea (green and black curves in Fig. (**3b**)) are about twice as large as those over land (green and black curves in Fig. (**3c**), note the different units in Fig. **3b**,**c**). A closer look at the compensation between NLW and $H_L$ reveals some dependence on the scenarios. By the end of the 21st century, the globally averaged value of $H_L$ and NLW in scenario A2 are about -6 W/m$^2$ and 7.7 W/m$^2$ (Table **2**), indicating that $H_L$ 'accounts' about 78% of the warming effect of NLW. This number changes to about 88% and 95% in scenario A1B and B1 (Table **2**). The result suggests that the compensation of the decrease in upward NLW through an increase in upward $H_L$ is less efficient in a scenario with higher GHG concentration. In other words, as the increase in GHG concentration becomes faster from B1, to A1B and to A2 scenario, the direct response, namely the decrease in upward NLW, becomes less and less compensated by the increase in upward $H_L$, leading to an acceleration of the warming.

Fig. (**3**) shows also that the responses in solar radiation NSW (blue) and $H_S$ (red) have opposite signs over land and over ocean. For the sensible heat flux, one finds an increase in downward $H_S$ over ocean (red curves in Fig. (**3b**)), but an increase in upward $H_S$ over land (red curves in Fig. (**3c**)). For the solar radiation, one finds a reduction in downward NSW over sea (blue curves in Fig. (**3b**)), but an increase in downward NSW over land (blue curves in Fig. (**3c**)). Thus, the warming effect of the decreased upward long wave radiation is enhanced by the sensible heat flux but suppressed by the solar radiation over sea, whereas the opposite is true over land. Due to the different roles of $H_S$ and NSW over land and sea, the two fluxes contribute little to the global averages.

Another difference between land and ocean concerns the evolution of the balance over time. Different from Fig. (**3b**)), in which NLW and $H_S$ are balanced by NSW and $H_L$ throughoutly, the balance over land changes with time in Fig. (**3c**)). Until about 2050, NSW, $H_L$ and $H_S$ contribute equally to balance the changes in NLW. After this there is a dramatic change in the NSW contribution such that it changes sign and the balance is maintained through almost equal but increasing contributions from $H_L$ and $H_S$.

a)

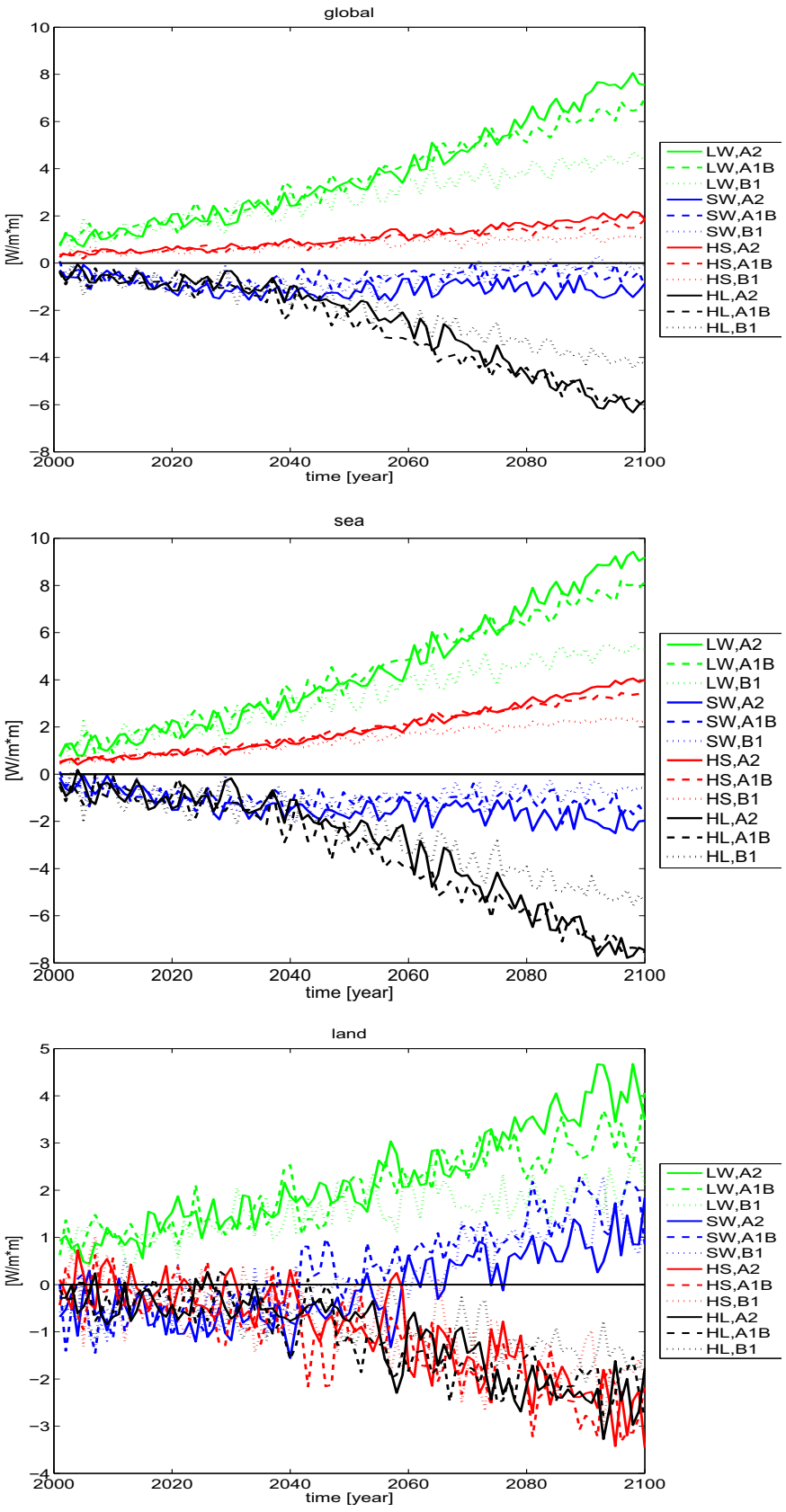


**Fig. (3).** Yearly time series of (**a**) globally averaged, (**b**) ocean-area averaged and (**c**) land-area averaged responses in long wave radiation (green), short-wave radiation (blue), sensible heat flux (red) and latent heat flux (black) in W/m$^2$, obtained from the A2 (solid), A1B (dashed) and B1 (dotted) scenarios. The time series represent the ensemble mean over the 21th century, relative to the respective time mean and ensemble mean in the 20th century.

The following sections consider effects and feedbacks affecting the NSW, $H_S$ and $H_L$ in more detail.

## 4. EFFECTS AND FEEDBACKS AFFECTING SHORT-WAVE RADIATION

The responses of short-wave radiation can be affected by various effects and feedbacks. Feedbacks can be studied by considering a simplified vertically-integrated energy balance equation [10, 11]. The present study is based on an ad-hoc analysis of surface variables. The effects of aerosol, the sea-ice albedo feedback, and the cloud feedback will be considered.

### a) The Aerosol Effect

In the ECHAM5 model, the direct effect of aerosols is parameterized. An increase in aerosols leads to a stronger absorption and scattering of short-wave radiation, which can result in a decrease in downward NSW at the surface. Thus, one way to assess the role of aerosols is to compare the time evolution of the sulfate concentration, which is shown in Fig. (**4**), with that of NSW, which is plotted again in Fig. (**5**) together with the clear-sky short-wave radiation ($NSW_{csky}$) to eliminate the effect of clouds.

Fig. (**5**) shows a decrease in NSW (blue) and $NSW_{csky}$ (red) for the first two decades of the 21st century. This corresponds well to the increase in sulfate concentration shown in Fig. (**4**). The decrease in B1 is weaker than A1B and A2, in particular for $NSW_{csky}$, consistent with the stronger increase in sulfate concentration in A1B and A2 than in B1. During the second half of the 21st century, the sulfate concentration decreases with time (Fig. **4**). The evolutions of NSW are notably different from those of $NSW_{csky}$, suggesting that cloud effects set in more clearly. When concentrating on $NSW_{csky}$, the decrease in sulfate concentration in the second half of the 21st century does result in a slight increase in $NSW_{csky}$ in B1-scenario (red dotted), but there is no notable increase in A1B- and A2-scenario (red dashed and solid lines). On the contrary, there is a further decrease by the end of the 21st century in A1B- and A2-scenario. It appears that the direct aerosol effect dominates only in the first two decades. Afterwards, the strong increase in water vapor in A1B- and A2-scenario can result in a strong reduction in NSW due to absorption of NSW, which is included in the ECHAM5 radiation scheme. The high concentrations of GHG gases by the end of the 21st century may lead to a further reduction in in NSW due to absorption of NSW.

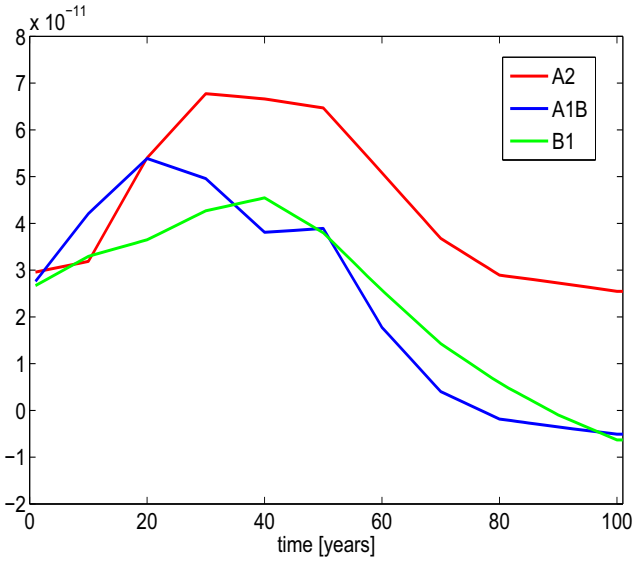


**Fig. (4).** Yearly time series of the area averaged sulfate burden in kg S/kg in A2 (red), A1b (blue) and B1 (green) scenario in the 21st century, relative to the mean values in the 20th century.

### b) The Sea-Ice Albedo Feedback

The response of NSW in climate change experiments can be affected by the positive feedback between temperature, sea-ice and albedo: An increase in GHG concentration leads to a decrease in upward NLW and a surface warming. The

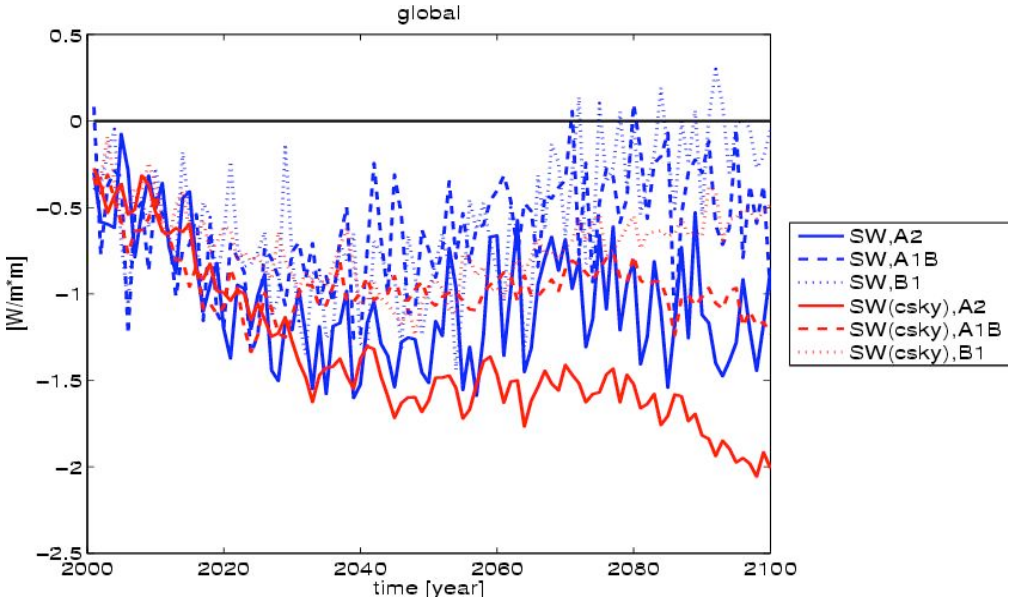


**Fig. (5).** Yearly time series of globally averaged short-wave radiation (blue) and clear-sky short wave radiation (red), obtained in the A2 (solid), A1B (dashed) and B1 (dotted) scenarios. The time series are derived in the same way as those in Fig. (**3**).

latter triggers the sea-ice retreat and from that a decrease in albedo and an increase in downward NSW. Such a change in NSW favors a further warming and a further retreat of sea ice.

Differences in 20-year means for sea ice cover (not shown) reveals the notable retreat of annual sea ice in the Arctic and along the Antarctic coast. Related to that, albedo is reduced in regions polward of the 20th century sea-ice margin (Fig. **6a**), with the largest amplitude reaching about 0.5. Again the signal is strongest in the A2-scenario, but has the same spatial structure in the other two scenarios. Over regions with large albedo reduction, an increase in downward NSW is found (Fig. **1b**). Moreover, the increase in near

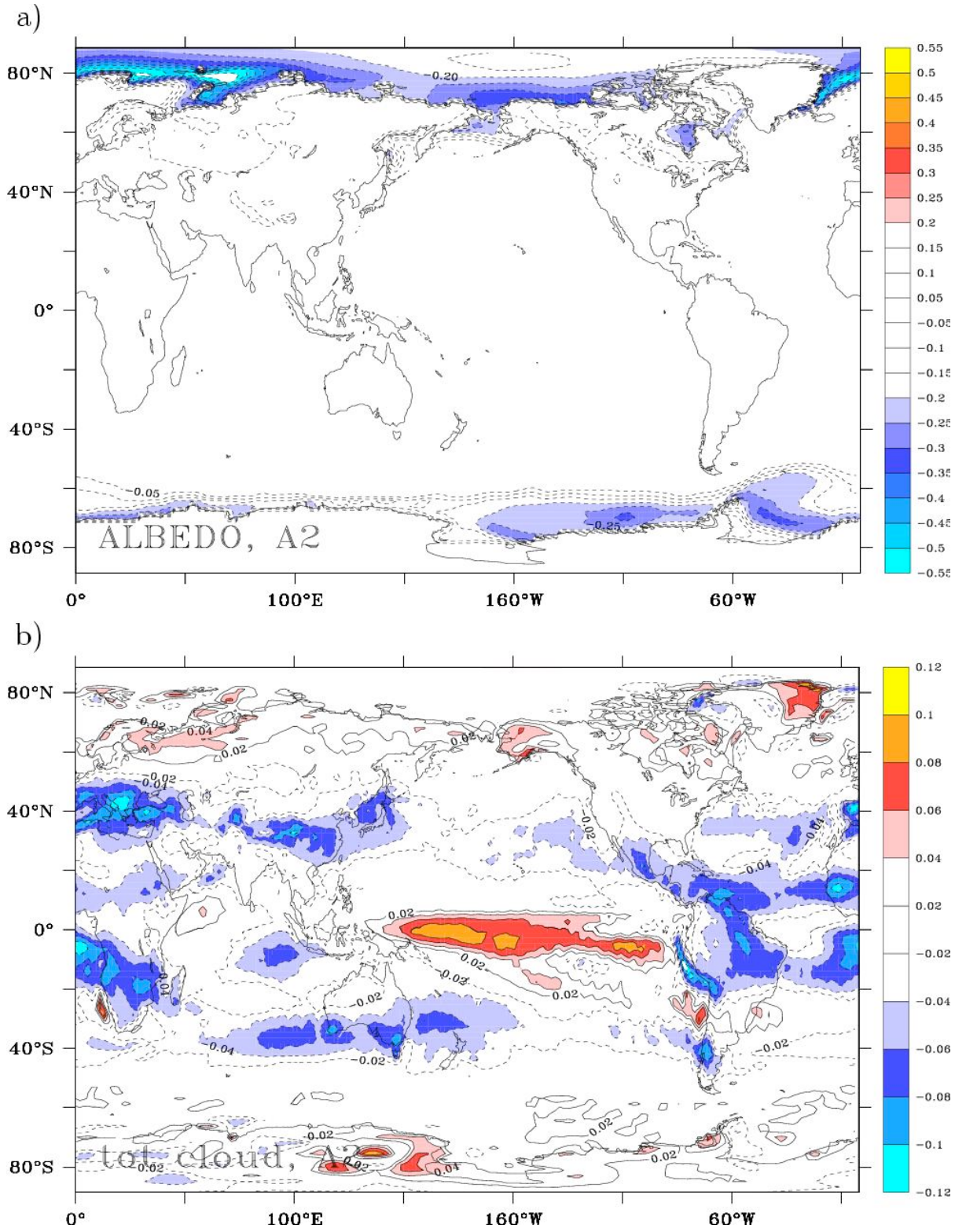


**Fig. (6).** As Fig. (**1**), but for (**a**) albedo and (**b**) total cloud cover. Both the albedo and the total cloud cover are values between 0 and 1.

surface air temperature is greater over these regions than further equatorward (not shown). The result suggests that the sea-ice albedo feedback does play a major role for the response in short-wav radiation.

**c) The Cloud Feedbacks**

The cloud feedback is more complicated. Over sea, a warming due to an increase in GHG concentration can lead to an increase in evaporation and cloud formation. The latter reduces the downward NSW at the surface and results in a weakening of the initial warming, leading to a negative feedback. The situation could be different over land where the water reservoir is limited. There, an increase in GHG concentration can result in dry conditions that suppresses evaporation and cloud formation. The latter allows an increase in NSW that strengthens the initial warming, leading to a positive feedback.

Fig. (**6b**) shows the difference in 20-year mean for the total cloud cover which represents the cloud area fraction. Over many land regions, such as central America, the southern part of the African continent and southern part of Australia, and also over the Mediterranean, there is a reduction in cloud cover. This reduction coincides with the increase in downward NSW in Fig. (**1b**). However, a comparison with near-surface temperature changes (not shown) suggests that even though the reduction in cloud formation tends to develop parallel to an increase in NSW, the increased NSW does not necessarily produce a large increase in surface temperature. For instance, the increase in NSW over Mediterranean does not lead to a large increase in surface temperature there (not shown). This suggests that a warming due to an increase in GHG concentration can trigger changes in cloudiness that alters the response of NSW. However, this response does not necessarily significantly feed back to the initial warming.

Over the tropical Pacific south of the equator, the increase of cloudiness corresponds to the reduction of NSW. The near-surface temperature reveals a weaker warming in the tropical Pacific south of the equator than north of the equator (not shown). This suggests that an increase in GHG concentration can trigger an increase in cloud formation that reduces downward NSW and consequently reduces the initial warming, leading to a negative feedback.

Fig. (**1b**) shows also notable reduction in downward NSW over the Southern Ocean, the North Pacific and the North Atlantic. This reduction is not related to large changes in total cloud cover. An inspection of the vertically integrated cloud water and the total precipitation (not shown) suggests that changes in NSW over the high-latitude oceans are likely caused by the large increases in the total amount of liquid water, rather than just by the increase in the total cloud cover.

**d) A Quantification of Different Effects**

The above analysis shows that different effects and feedbacks are locked to different geographical regions. This suggests that the relative importance of the considered effects and feedbacks can be assessed by averaging NSW over selected geographic regions. For instance, the sea-ice albedo feedback can be quantified by averaging NSW over regions polward of the 20th century sea-ice margin, where albedo changes pass a prescribed threshold. The cloud effect can be quantified by averaging NSW over regions where changes in total cloud cover pass a prescribed threshold. The relative amplitudes of the two conditioned area averages can indicate the relative strengths of the two effects.

Obviously, the conditioned area averages are only efficient in determining the importance of different feedbacks when the selected areas do not overlap. To avoid overlapping, the thresholds used to define the areas should not be too small. On the other hand, the values obtained depend crucially on the thresholds used. Thus, the conditioned area averages are only very crude quantifiers. This should be kept in mind when interpreting the results.

Fig. (**7**) shows that the effect of albedo leads to the largest area-averaged changes in NSW. However, since the area affected by the albedo feedback is small, the sea-ice albedo effect (red), which reaches the estimated amplitude of about 12 $W/m^2$ by the end of the 21st century in the A2-scenario, does not dominate the total response of NSW (blue curve in Fig. (**3a**)). Relative to the sea-ice albedo effect, the effects of the total cloud cover, the precipitation and cloud water are much weaker. Over ocean, they reach comparable amplitudes. Over land, the cloud cover is more important for changes in NSW. In particular, the increase in NSW averaged over areas with a reduction in cloud cover can reach about 6 $W/m^2$ (blue curve in Fig. (**7b**)). This increase could contribute to the total mean response of NSW over land (blue curve in Fig. (**3c**)).

It is noted that over land, areas with large precipitation changes overlap partially with the areas of large cloud cover changes, despite the fact that relative large thresholds are chosen for conditioned area averages. There are also overlapping areas between precipitation and cloud water over ocean areas. Thus, total response in NSW (black) is generally not the sum of responses due to different effects, as suggested by the conditional area averages.

Note also that the cloud water effect over land (green curve in Fig. (**7b**)) is caused by large increases in cloud water content over the northern part of North America and Eurasia (not shown). The effect of cloud water content is estimated to be up to about 3 to 4 $W/m^2$ (green line in Fig. (**7b**)), which is smaller than the effect related to the increase in cloud cover in the land regions further equatorwards which leads to the blue line in Fig. (**7b**). The increase in cloud water over the northern part of North America and Eurasia, is also related to an increase in cloud cover and precipitation. However, the magnitudes of the latter are smaller than the threshold chosen for the calculation of the conditioned area averages. One can conclude that the green line indicates the effect of cloud water content on NSW over the northern part of North America and Eurasia, whereas the blue and magenta lines describe the cloud cover and precipitation effects on NSW over land areas further equatorward.

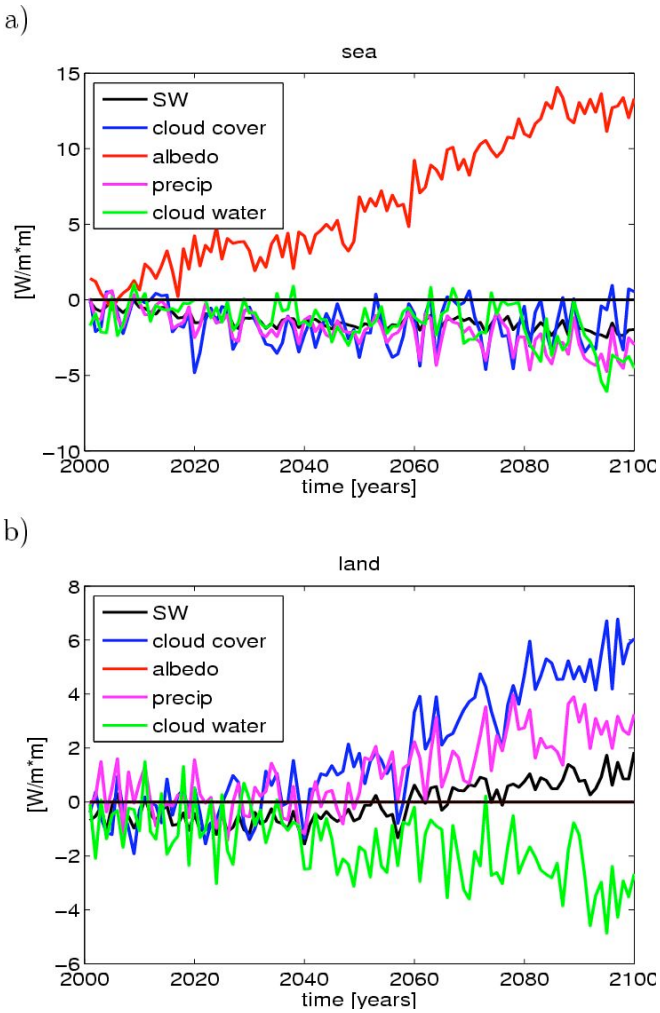


**Fig. (7).** Conditioned averages over land (bottom) and sea (top) areas. The thresholds used to calculate the conditional averages are 0.3 for albedo, 0.05 for total cloud cover, 0.6 10-5 kg/(m$^2$s) for precipitation and 0.04 kg/m$^2$ vertically integrated cloud water.

## 5. EFFECTS AFFECTING SENSIBLE HEAT FLUX

The sensible heat flux is determined by the difference in air temperature and surface temperature. To understand the change in $H_S$, the change of $T_{2m}$-$T_s$ in the last two decades of the 21$^{st}$ century (2080-2099) relative to that in the first two decades of the 20th century (1900-1919) is considered, where $T_{2m}$ indicates the 2-meter temperature and $T_s$ the surface temperature. $T_s$ equals SST over sea.

The difference map for $T_{2m}$-$T_s$ (Fig. **8**) reveals two striking features. First, $T_{2m}$-$T_s$ is increased over most of the ocean areas, but tends to be negative over land, in particular over the northern part of Eurasia and North America. The result suggests that the air is warmer than the surface over the oceans and mostly cooler than the surface over land. This behavior is likely caused by the different heat capacity of soil and water. Soil with a smaller heat capacity can be more easily warmed up than the ocean. The land-sea contrast in Fig. (**8**) corresponds well to that in Fig. (**2a**). This suggests that the different responses of $H_S$ over land and sea result from different changes in the air-surface temperature difference $T_{2m}$-$T_s$.

Secondly, large negative values of $T_{2m}$-$T_s$ are found near the edge of the present-day sea-ice distribution (z.B. near 80$^o$N). As sea-ice migrates polwards by the end of the 21st century in A2-scenario, the oceans in the formerly ice covered areas are more often exposed to colder air, leading to the large increase in upward $H_S$ as sea ice retreats (Fig. **2a**). However, this effect is, at least when integrated globally, weaker than the increase in downward $H_S$ over oceans due to the increase in $T_{2m}$-$T_s$.

## 6. EFFECTS AND FEEDBACKS AFFECTING LATENT HEAT FLUX

The overall increase in upward latent heat flux in Fig. (**2b**) is clearly related to the water vapor feedback: An increase in GHG concentration enhances the downward NLW, leading to a warming of the surface. The latter favors evaporation and produces an increase in upward latent heat flux. The increase in water vapor in turn further strengthens the downward NLW and upward latent heat flux, resulting in a positive feedback.

Due to the water vapor feedback, the decrease in upward NLW is largely balanced by the increase in upward latent heat flux. However, there are a few exceptions. The most prominent one is that over the North Atlantic, where an increase of downward latent heat flux is found and changes in NLW and $H_L$ reinforce, rather than compensate each other. Consequently, the change of the total flux (i.e. NLW+NSW+$H_S$+$H_L$) has the largest values of about 50 W/m$^2$ over the North Atlantic. This heat flux change is likely responsible for the weakening of the Atlantic meridional overturning circulation (AMOC) in the 21st century.

Why does the latent heat flux behave so differently over the North Atlantic? The latent heat flux is calculated using the bulk formula,

$$HL = C\rho \mid v_l \mid (q_l - q_s) \qquad (3)$$

where C is the transfer coefficient. $v_l$ is the horizontal wind vector at the lowest model level l. $q_l$ and $q_s$ are specific humidity at level l and at the surface, respectively. According to Eq.(3), there are two ways to obtain a reduction in latent heat flux, namely by a reduction of the vertical contrast $q_l$-$q_s$, or by a reduction of the wind speed.

The difference map for the change in the wind speed (not shown) displays a large increase of wind speed over the Southern Ocean. Over the North Atlantic, the changes are much smaller. Around 55$^o$N to 60$^o$N, where the reduction in upward latent heat flux is found, the wind speed is even increased by the end of the 21$^{st}$ century. Thus, the wind speed change is not the cause for the reduction in upward latent heat flux.

Here we denote the changes in the low-level specific humidity and surface saturation humidity by $\Delta q_l$ and $\Delta q_s$, respectively. In a warming climate, both $\Delta q_l$ and $\Delta q_s$ will be positive. In case of no change in wind speed, the change in latent heat flux is proportional to $\Delta q_l$-$\Delta q_s$. Since $q_s$ is proportional to the saturation pressure $e_s$, $q_s$ must be, according to the Clausius-Claperyon equation, proportional to exp(-a/$T_s$)

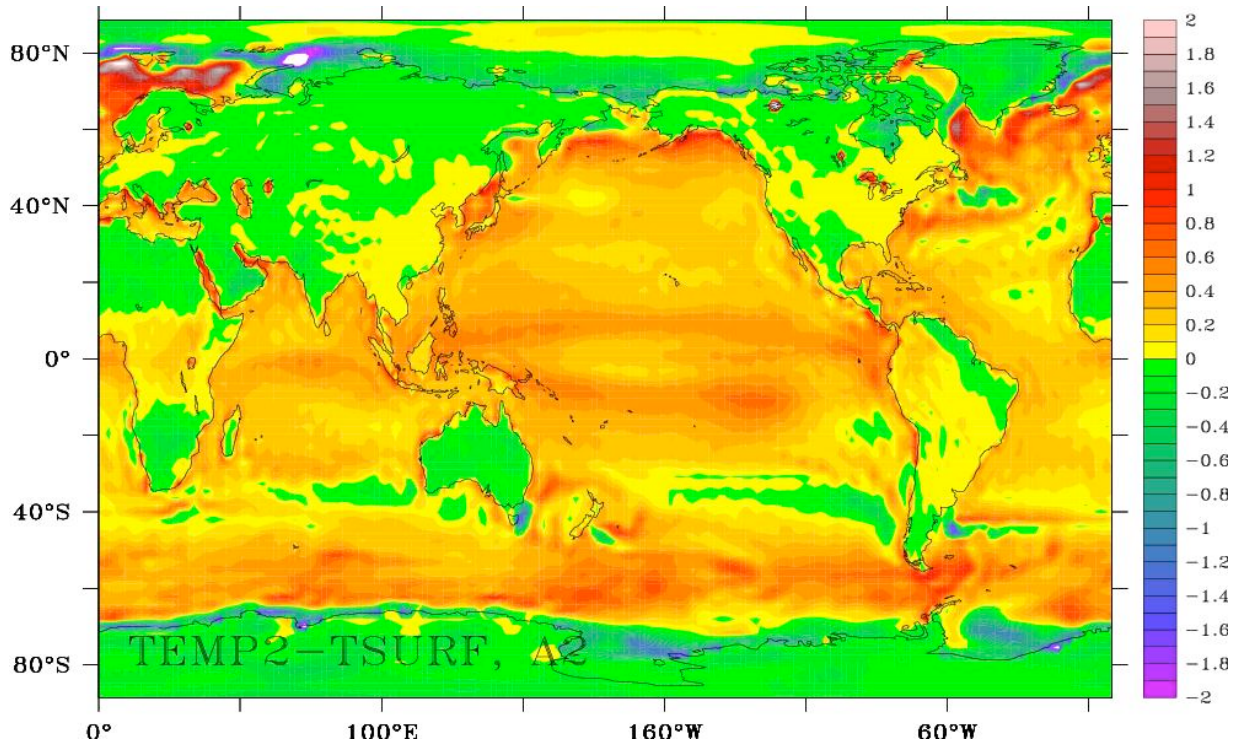


**Fig. (8).** Same as Fig. (**1**), but for the air-surface temperature difference $T_{2m}$-$T_s$, where $T_{2m}$ represents 2m air temperature and $T_s$ the surface temperature which is identical to SST over ocean.

with a being a constant and $T_s$ being the SST. The amplitude of $\Delta q_s$ hence depends on the changes in SST. Assume that $\Delta q_l$ does not vary too much from ocean basin to ocean basin, which is consistent with the distribution of low-level specific humidity changes. The contrast between the North Atlantic and other regions shown in Fig. (**2b**) is only possible when $\Delta q_s$ is smaller than $\Delta q_l$ in the North Atlantic, but larger than $\Delta q_l$ outside the North Atlantic.

SST changes in the North Atlantic can be smaller than elsewhere, due to downward propagation of the surface warming *via* advection induced by the AMOC. As a result, the change in specific humidity $\Delta q_s$ will be smaller over the North Atlantic than elsewhere. Thus, the exceptional position of $H_L$ in the North Atlantic is likely directly coupled to the downward branch of the AMOC.

If this is correct, a reduction of upward latent heat flux over the North Atlantic should also be produced by IPCC integrations performed with other coupled models. To check this, latent heat flux data in the 20th century and in the 21st century in A2-scenario, that are produced by nine different coupled models, including those from climate research centers such as NCAR, GFDL and the UK Met Office, are extracted from the IPCC data distribution center. Indeed, all nine models simulate a reduction of upward latent heat flux over the North Atlantic. The amplitude of the reduction ranges from 15 to 25 W/m$^2$.

As being directly coupled to the AMOC, the reduction of upward latent heat flux in the North Atlantic represents a coupled phenomenon. The reduction provides more downward heat flux over the North Atlantic than elsewhere and is likely responsible for the weakening of the Atlantic MOC.

## 7. CONCLUDING REMARKS

The response of surface fluxes to an increase in GHG concentration is analyzed using the IPCC AR4 climate change experiments with the ECHAM5/MPI-OM coupled model. The analysis concentrates on the changes in NSW, $H_S$ and $H_L$. Similar in the previous studies, the decrease in upward long wave radiation due to an increase in GHG concentration is largely compensated by an increase in upward latent heat flux, which results from an increase in evaporation. However, there are two new aspects, which could not be described by the earlier 2x$CO_2$-experiments using AGCMs coupled to a mixed layer ocean model. The first aspect concerns the degree of compensation. It is found that the offset of NLW by $H_L$ decreases from scenario B1, which has the slowest rate of increase in GHG concentration, to scenario A1B and A2, in which the GHG concentration increases much faster. It seems that the degree of compensation decreases with increasing rate of change of the GHG concentration. The second aspect concerns the spatial distribution of compensation. Even though the compensation takes place almost everywhere, a few exceptions do exist. The most striking one occurs in the North Atlantic, where total surface heat flux is strongly increased due to reduced upward NLW *and* a reduction in upward $H_L$. The latter can result from vertical advection of heat through the Atlantic MOC which cannot be simulated with a mixed layer model. This change in total surface heat flux is likely the cause for the weakening of the Atlantic MOC in the 21st century.

## ACKNOWLEDGEMENT

This work is supported by the *Deutsche Forschungsgemeinschaft* through the project SFB-512. Thanks also the colleagues from MPI and DKRZ for performing the IPCC integrations. We thank Stephan Bakan for helpful discussions.

## REFERENCES

[1] Gutowski, WJ Gutzler DS, Wang WC. Surface energy balances of three general circulation models: implications for simulating regional climate change. J Climate 1991; 4: 121-134.

[2] Boer GJ. Climate change and the regulation of the surface moisture and energy budgets. Clim Dyn 1993; 8: 225-239.

[3] Watterson IG, Dix MR. Influences on surface energy fluxes in simulated present and doubled $CO_2$ climates. Clim Dyn 1996; 12: 359-370.

[4] Wild M, Ohmura A, Cubasch U. GCM-simulated surface energy fluxes in climate change experiments. J Climate 1997; 10: 3093-3110.

[5] Garratt JR, O'Brien DM, Dix MR, Murphy JM, Stephens GL, Wild M. Surface radiation fluxes in transient climate simulations. Glob Planet Change 1999; 20: 33-55.

[6] Roeckner E, and co-authors. The atmospheric general circulation model ECHAM5, Part I: Model description. Max-Planck-Institut für Meteorologie Rep 2003; 349, 127pp.

[7] Marsland SJ, Haak H, Jungclaus JH, Latif M, Roeske F. The Max-Planck-Institute global ocean/sea ice model with orthogonal curvilinear coordinates. Ocean Model 2003; 5: 91-127.

[8] Jungclaus J, Keenlyside N, Botzet M, *et al.* Ocean circulation and tropical variability in the coupled model ECHAM5/MPI-OM. J Climate 2006; 3952-3972.

[9] Wild M, Ohmurra A, Gilgen H, Roeckner E, Giorgetta M, Morcrette JJ. The disposition of radiative energy in the global climate system. Climate Dyn 1998; 14, 853-869.

[10] Watterson IG, Dix MR, Colman RA. A comparison of present and doubled $CO_2$ climates and feedbacks simulated by three general circulation models. J Geophy Res 1999; 104: 1943-1956.

[11] Watterson IG, Dix MR. Effective sensitivity and heat capacity in the response of cloamte models to greenhous gas and aerosol forcings. Q J R Meteorol Soc 2005; 131: 259-279.

Received: April 7, 2008 Revised: May 2, 2008 Accepted: May 8, 2008